Journal of Materials Chemistry C

Accepted Manuscript

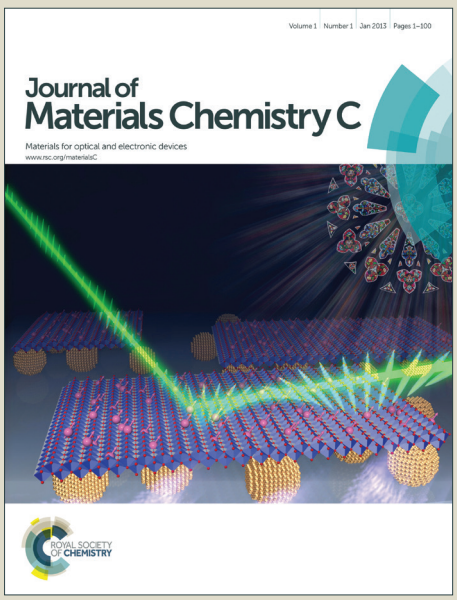

ROYAL SOCIETY OF CHEMISTRY

www.rsc.org/materialsC

Generation of orange and green Emissions in $Ca_2GdZr_2(AlO_4)_3:Ce^{3+},Mn^{2+},Tb^{3+}$ Garnet via Energy Transfer with Mn^{2+} and Tb^{3+} as Acceptors

Wei Lü[a,*], Wenzhen Lv [a,b], Qi Zhao [a,b], Mengmeng Jiao [a,b], Baiqi Shao [a,b] and Hongpeng You[a,*]

[a]State Key Laboratory of Rare Earth Resource Utilization, Changchun Institute of Applied Chemistry, Chinese Academy of Sciences, Changchun 130022, P. R. China.

[b] University of the Chinese Academy of Sciences, Beijing 100049, P. R. China.

*Corresponding author: E-mail address: hpyou@ciac.ac.cn;wlv@ciac.ac.cn.

Fax: +86-431-85698041; Tel: +86-431-85262798;

Abstract: Utilizing Mn^{2+} and Tb^{3+} ions as energy-transfer acceptors, we report a series of emission color-tunable $Ca_2GdZr_2(AlO_4)_3:Ce^{3+},Mn^{2+},Tb^{3+}$ aluminate garnets. Incorporating Mn^{2+} and Tb^{3+} into $Ca_2GdZr_2(AlO_4)_3:Ce^{3+}$ phosphor generates an orange emission band peaking at 572 nm and a green line peaking at 550 nm. The energy transfer from Ce^{3+} to Mn^{2+} and Ce^{3+} to Tb^{3+} ions are deduced from the spectral overlap between Ce^{3+} emission and Mn^{2+}/Tb^{3+} excitation spectra. Fluorescence decay patterns are studied as a function of Mn^{2+} and Tb^{3+} concentrations. The calculated values based on the luminescence dynamical process indicates that the intensity ratios of orange to green band as a function of Mn^{2+} concentrations are in good agreement with that obtained directly from emission spectra. Commission on illumination value of color tumble emission as well as luminescence external quantum yield (20.4−48.9%) can be tuned by precisely controlling the content of Ce^{3+}, Mn^{2+}, and Tb^{3+}. The energy transfer significantly enables the achievement of a broad emission spectrum covering an orange spectral region. It is suitable for a near-UV light-emitting diode (LED) excitation.

1. Introduction

The light-emitting diodes (LEDs)-based white light sources have received increasing interest in recent years for their promising applications such as automotive displays, and solid-state lighting due to lower energy consumption, good reliability, long lifetime and environmental protection[1-4]. At present, commercial white LED based on YAG:Ce^{3+} phosphor exhibits a poor color rendering index (CRI ≈ 70-80) and a high correlated color temperature (CCT ≈ 7750 K) because of lacking a red-light contribution.[5-7] Recently, white light conversion from near-UV light emitting diodes (NUV-LEDs) by use of tricolor phosphors are considered to be a more promising route to cover indoor lighting needs for their better color rendering ability.[8-20] In this regard, it is important to develop new high efficient phosphors for NUV-LEDs applications.

It has been well known that Ce^{3+} ion exhibits good performances for its special optical properties of a broad band emission ranging from green to red in many different material hosts. Especially Ce^{3+} activated garnet phosphors with formula unit of $L_3D_2(AO_4)_3$ such as $Y_3Al_5O_{12}:Ce^{3+}$ (YAG:Ce^{3+}),[21] $Lu_2CaMg_2(SiO_4)_3:Ce^{3+}$ and $Ca_3Sc_2Si_3O_{12}:Ce^{3+}$,[22,23] which are used as visible phosphors in conventional white LEDs, all exhibit highly efficient down-conversion luminescence. Furthermore, additional red-emitting centers are introduced into the $L_3D_2(AO_4)_3$ system to compensate the red spectral deficiency. For example, Mueller-Mach et al. added Pr^{3+} into YAG:Ce^{3+} and consequently obtained a red emission line at 608 nm or Jia et al. created additional red emission via incorporating Mn^{2+}–Si^{4+} into the YAG:Ce^{3+} lattice.[24,25] Liu et al. realized a full color emission by co-doping Ce^{3+} and Mn^{2+} into a single $Ca_3Sc_2Si_3O_{12}$ host and demonstrate the adjustment of the color quality through the addition of doped Ln (Ln = La, Gd, Lu and Y) ions.[26,27]

Recently, Gong et al. reported a novel garnet-structure $Ca_2GdZr_2(AlO_4)_3:Ce^{3+}$ phosphor.[28] Its

excitation spectrum covers the NUV and blue regions, and this phosphor can produce a very broad emission band that peaks at 510 nm. Thus, it is expected that $Ca_2GdZr_2(AlO_4)_3:Ce^{3+}$ may produce longer wavelength visible emission by codoping acceptors into the same crystalline matrix using the principle of energy transfer. In this work, we tentatively introduce Tb^{3+} and Mn^{2+} into $Ca_2GdZr_2(AlO_4)_3:Ce^{3+}$. Utilizing energy transfer, the Tb^{3+} and Mn^{2+} ions can give rise to a green line peaking at 542 nm and an orange emission band peaking around 570 nm in the present work. Energy transfer from Ce^{3+} to Tb^{3+} and Ce^{3+} to Mn^{2+} in $Ca_2GdZr_2(AlO_4)_3$ is systematically investigated by the photoluminescence excitation and emission spectra, and lifetimes. Quantum yields and CIE chromaticity coordinates of $Ca_2GdZr_2(AlO_4)_3:Ce^{3+}$, Mn^{2+},Tb^{3+} are also studied.

2. Experimental Section

The $Ca_{2-y}Gd_{1-x-z}Zr_2(AlO_4)_3:xCe^{3+},yMn^{2+},zTb^{3+}$(abbreviated as $CGZA:xCe^{3+},yMn^{2+},zTb^{3+}$; Mn^{2+} substitutes for Ca^{2+}, Ce^{3+} and Tb^{3+} substitute for Gd^{3+}, where the x, y and z are mole percent) phosphors were synthesized by a high-temperature solid-state reaction. The constituent oxides or carbonates $CaCO_3$ (A.R. (Analytical Reagent)), Al_2O_3 (A.R.), ZrO_2(99.99%), Gd_2O_3(99.99%), CeO_2 (99.99%), Tb_4O_7 (99.99%), and $MnCO_3$ (A.R.) were employed as the raw materials, which were mixed homogeneously by an agate mortar for 30 minutes, placed in a crucible with a lid, and then sintered in a tubular furnace at 1550°C for 4 h in reductive atmosphere (10% H_2 + 90% N_2 mixed flowing gas).

The structure of the sintered samples was identified by powder X-ray diffraction (XRD) analysis (Bruker AXS D8), with graphite monochromatized Cu Kα radiation (λ = 0.15405 nm) operating at 40 kV and 40 mA. The measurements of photoluminescence (PL) and photoluminescence excitation (PLE) spectra were performed by using a Hitachi F4500 spectrometer

equipped with a 150 W xenon lamp under a working voltage of 700 V. The diffuse reflectance spectra were obtained using a Hitachi U-4100 spectrophotometer with the reflection of black felt (reflection 3%) and white Al_2O_3 (reflection 100%). External photoluminescence quantum yields (QYs) were measured by using the absolute PL quantum yield measurement system (C9920-02, Hamamatsu Photonics K. K., Japan). The luminescence decay curve was obtained from a Lecroy Wave Runner 6100 digital oscilloscope (1GHz) using a tunable laser (pulse width = 4 ns, gate = 50 ns) as the excitation source (Continuum Sunlite OPO).

3. Results and Discussion

3.1. Phase Identification

The incorporation of Ce^{3+}, Mn^{2+}, Tb^{3+} ions in the crystal lattice of CGZA is examined by XRD analysis. Figure 1 presents the XRD patterns of the CGZA:Ce^{3+},Mn^{2+} and CGZA:Ce^{3+},Tb^{3+} samples. All the diffraction peaks are well indexed to those of the reported $Ca_2GdZr_2(AlO_4)_3$ phase. The doping of lanthanide and transition metal ions does not induce any other distinct impurities phases, indicating the successful incorporation of these activators into the CGZA host. Previous reported works demonstrated that Ca^{2+} has been introduced into the L sites with Zr^{4+} introduced to the D sites in $L_3D_2(AO_4)_3$, giving a garnet structure of $Ca_2GdZr_2(AlO_4)_3$.[28] In the structures of this compound, Ca^{2+} and Gd^{3+} ions occupy the L sites with a ratio of 2:1 and are both in eight-coordinated dodecahedron. Zr^{4+} and Al^{3+} are octahedral and tetrahedral coordinated, respectively. The oxygen atoms form bridges between [ZrO_6] octahedrons and [AlO_4] tetrahedral. Basing on the effective ionic radii (r) of cations, Tb^{3+} ions are expected to occupy Gd^{3+} sites because the ionic radius of Tb^{3+} (1.04 Å for CN = 8) is close to that of Gd^{3+}(r = 1.05 Å for CN = 8). Accounting for ion valence, we presume that Ce^{3+} (r = 1.14 Å for CN = 8) and Mn^{2+}(r = 0.96 Å for CN = 8) are expected to occupy

the sites of Gd^{3+} and Ca^{2+} (r = 1.12 Å for CN = 8) preferably.

3.2. Luminescent Properties of CGZA:Ce^{3+},Mn^{2+}

Figure 2 shows the PL and PLE spectra of CGZA:Ce^{3+} and CGZA:Mn^{2+} phosphors together with the reflection spectra of CGZA and CGZA:Ce^{3+} samples. The PLE spectrum of CGZA:Ce^{3+} clearly demonstrates that there are several broad absorption bands peaked at 260, 340, 420 nm, which can also be validated by the diffuse reflection spectra of CGZA and CGZA:Ce^{3+} samples. Upon excitation of 420 nm, the CGZA:Ce^{3+} phosphor exhibits an intense green luminescence, which is assigned to the electric-dipole-allowed transition from the lowest level of the 5d excited state to the 4f ground state of the Ce^{3+} ions. Compared to the PL spectrum of CGZA:Ce^{3+}, CGZA:Mn^{2+} shows a very weak emission upon UV light excitation due to forbidden f-f absorption transitions of Mn^{2+} in UV. The excitation spectrum of CGZA:Mn^{2+} phosphor consists of several bands centered at 375 and 458 nm, which are assigned to the transitions from the $^6A_1(6S)$ to $^4T_2(4D)$ and $^4T_2(^4G)$ levels of the Mn^{2+} ions, respectively.[29] The comparison of the PL spectra for CGZA:Ce^{3+} and the PLE spectrum for CGZA:Mn^{2+} reveals a great spectral overlap between the emission band of Ce^{3+} and the Mn^{2+} excitation transitions. This indicates that energy transfer from Ce^{3+} to Mn^{2+} may occur in CGZA. Figure 3 illustrates the PLE and PL spectra of CGZA:Ce^{3+},Mn^{2+}. The PLE spectrum monitored by the 570 nm emission of the Mn^{2+} is similar to that is monitored by the green emission of Ce^{3+}. This phenomenon demonstrates the existence of energy transfer from Ce^{3+} to Mn^{2+}. Figure 4 illustrates a series of the emission spectra for CGZA:Ce^{3+},Mn^{2+} (y=0, 0.04, 0.08, 0.12, 0.16, 0.20 and 0.24) under near UV excitation (λ_{ex} =420 nm). With increasing Mn^{2+} concentration, the emission intensities of the Mn^{2+} increase followed by the decrease of Ce^{3+} emission intensities, reflecting the result of energy transfer from Ce^{3+} to Mn^{2+}.

In order to investigate the luminescence dynamics, the fluorescence lifetimes τ_1 for Ce^{3+} with different Mn^{2+} concentrations are measured and presented in Figure 5. In donor-acceptor energy transfer system, due to nonexponential decay of donor fluorescence intensity $I_D(t)$ in the presence of acceptors, we define an average fluorescence lifetime of the donors as

$$\tau_D = \int_0^\infty I_D(t)dt, \quad (1)$$

where $I_{D0}(t)$ is the decay function of donors in the absence of acceptors, which have normalized to its initial intensity. The energy transfer efficiency $\eta_{Ce\text{-}Mn}$ can be calculated using

$$\eta_{Ce\text{-}Mn} = 1 - \tau_1 / \tau_0 \quad (2)$$

where τ_0 is the lifetime of the Ce^{3+} ions in the absence of the Mn^{2+} ions and τ_1 is the lifetime of the Ce^{3+} ions in the presence of the Mn^{2+} ions. The calculated energy transfer efficiency is shown in Figure 6. The efficiency $\eta_{Ce\text{-}Mn}$ increases with increasing y and reaches 53.23 % at y = 0.24.

The remarkable enhancements of the orange band relative to green band are observed with increasing Mn^{2+} concentration. The fluorescence lifetimes of Ce^{3+} (τ_1) with different Mn^{2+} concentration in CGZA:Ce^{3+},Mn^{2+} phosphors are measured by monitoring at 500 nm with an irradiation of 340 nm. As shown in Figure 5, the fluorescence lifetimes of Ce^{3+} reduces with increasing Mn^{2+} concentrations, reflecting the characteristics of energy transfer between donors and acceptors. Based on energy transfer, the dependences of the emission intensity ratios of Mn^{2+} to Ce^{3+} on Mn^{2+} concentration are calculated by the measured fluorescence lifetimes of Ce^{3+}(τ_1) and Mn^{2+}(τ_2). Under steady excitation, the rate equations describing the energy transfers from Ce^{3+} to Mn^{2+} can be written as follows:

$$W_{Ce-Mn} n_1 = n_2 / \tau_2 \quad (3)$$

where n_1, and n_2 are the populations of Ce^{3+} and Mn^{2+} ions, respectively; The energy transfer rates

(W_{Ce-Mn}) can be obtained using the equation:

$$W_{Ce-Mn} = 1/\tau_1 - 1/\tau_0 \quad (4)$$

Since the fluorescence intensity of a specific level is equal to the product of the population and the radiative rate of the level, using Eq. (3), the dependences of the intensity ratio of the orange to green emissions on Mn^{2+} concentrations can be written as

$$\frac{I_O}{I_G} = \frac{n_2\gamma_2}{n_1\gamma_1} = \frac{W_{Ce-Mn}\gamma_2\tau_2}{\gamma_1} \quad (5)$$

where γ_1 and γ_2 are radiative rates of Ce^{3+} and Mn^{2+}, respectively, which are independent of Mn^{2+} concentrations. W_{Ce-Mn} has been calculated according to Eq.(2). τ_2 are determined to be 1.39, 1.29, 1.25, 1.10 1.12 and 1.07 ms for the CGZA:Ce^{3+},Mn^{2+} phosphors with y=0.04, 0.08, 0.12, 0.16, 0.20 and 0.24 respectively. Therefore, the intensity ratios I_O/I_G at various Mn^{2+} concentrations can be calculated using Eq. (5) and scaled to the maximum, as shown in Figure 7. For comparison, the intensity ratios obtained directly from the emission spectra are also given in Figure 7. It can be seen that the calculated data based on lifetimes are in good agreement with the experimental ones based on the PL spectra.

If the donor and acceptor ions are uniformly distributed in the host and the migration process are negligible compare to energy transfer between donors and acceptors. The normalized intensity of the donor fluorescence can be written as

$$I_D(t) = I_{D0}(t) f(t) \quad (6)$$

The function *f*(t) characterizes the loss of excited donors due to one way energy transfer to the acceptors. According to Inokuti - Hirayama formula, [30] we have

$$f(t) = \exp[-\frac{4}{3}\pi\ \Gamma(1-\frac{3}{m})n_A\alpha^{3/m}t^{3/m}] \quad (7)$$

Where α is a rate constant for energy transfer. m = 6, 8, 10, the coefficient for dipole-dipole, dipole-quadrupole, and quadrupole-quadrupole interaction, respectively. n_A is the number of acceptor ions per unit volume. From Eq.(6) and (7), $\log\{\ln[I_{D0}(t)/I_D(t)]\}$ acts as a linear function of $\log(t)$ with a slope of $3/m$. In order to well understand the Ce-Mn energy transfer process, we plot the $\log\{\ln[I_{D0}(t)/I_D(t)]\}$ vs $\log(t)$ for various samples. As shown in Figure 8, the value of S estimated from the slope is found to be 5.80, 6.10, and 5.92 for CGZA:Ce^{3+},yMn^{2+} samples with y = 0.04, 0.08, and 0.12, respectively. These values are nearly coincident with the conventional value of m = 6, indicating that the dominant interaction mechanism for CGZA:Ce^{3+},Mn^{2+} is based on the dipole-dipole interaction.[31-33]

3.3 Luminescent Properties of CGZA:Ce^{3+},Tb^{3+}.

Figure 9 shows the PL and PLE spectra of three samples, namely Ce^{3+} singly doped CGZA (a), Tb^{3+} singly doped CGZA (b), and Ce^{3+}, Tb^{3+} doubly doped CGZA (c), respectively. The PLE spectrum of Tb^{3+} consists of several lines in the region from 300 to 500 nm which correspond to absorption f–f transition of Tb^{3+} ion. The Tb^{3+} emission lines are located at 485, 550, 580, and 620 nm, which are assigned to the $^5D_4$ to ^7F_J (J = 6, 5, 4, 3) multiplet transitions, respectively. In Figure 9(c) the PL spectrum of Ce^{3+} and Tb^{3+} doubly doped sample contains not only the green band of Ce^{3+} but also the green lines of Tb^{3+} when only Ce^{3+} is excited at 420 nm. This phenomenon proves the occurrence of energy transfer from Ce^{3+} to Tb^{3+}. To further exam the energy transfer in the doubly doped sample, the PLE spectrum of the pure 550 nm green line can be obtained as follows: Since the PLE spectrum of the pure Ce^{3+} at 550 nm can be obtained by averaging that monitoring 530 nm and 570 nm (Figure 9(d) and (e)), After simple subtraction, we can finally obtain the individual PLE spectrum of pure 550 nm green line, as shown in Figure 9(f). It is clearly presented that the PLE

spectrum of the pure 550 nm emission line of Tb^{3+} is similar to the PLE bands of Ce^{3+}. The above analysis on the PLE and PL spectra of the CGZA:Ce^{3+},Tb^{3+} phosphor proves the occurrence of the energy transfer from the Ce^{3+} to Tb^{3+} ions.

Figure 10 shows the variation of PL spectra of Ce^{3+} and Tb^{3+} in the CGZA:Ce^{3+},Tb^{3+} samples with increasing Tb^{3+} doping concentrations. Under excitation at 420 nm, each of the emission spectrum for CGZA:Ce^{3+},Tb^{3+} samples consist of an emission band of Ce^{3+} ions and several emission peaks of Tb^{3+} ions. When the Tb^{3+} concentration (z) increases, the remarkable enhancements of the Tb^{3+} emission band relative to Ce^{3+} emission band are observed. The energy transfer efficiency (η) from the Ce^{3+} to Tb^{3+} ions in CGZA:Ce^{3+},Tb^{3+} is also calculated using the Eq.(2), as shown in Figure 11. The energy transfer efficiency of Ce^{3+} and Tb^{3+} shows that the energy transfer efficiency increases as the Tb^{3+} concentration increased. Figure 12 illustrates the relationships between $\log\{\ln[I_{D0}(t)/I_D(t)]\}$ versus $\log(t)$ using the Eq. (6) and (7), revealing a linear behavior when m=6. This implies that the energy transfer from sensitizer Ce^{3+} to activator Tb^{3+} also follows a nonradiative dipole- dipole mechanism.

3.4. Quantum yields and the Chromaticity of CGZA:Ce^{3+},Tb^{3+},Mn^{2+}.

The external quantum yields (QY) is an important parameter to be considered for practical LED application. Thus, the corresponding external QY values measured. Figure 13 gives the values of the relative intensity and the external quantum yields of CGZA:Ce^{3+},yMn^{2+} and CGZA:Ce^{3+}, zTb^{3+} samples. It is observed that the tendency of the absolute quantum yields is consistent with that of the relative intensity. For the CGZA:Ce^{3+},yMn^{2+} (y=0, 0.04, 0.08, 0.12, 0.16, 0.20 and 0.24) series samples, the external QY values decrease obviously with the increase of Mn^{2+} concentration, which should be in relation to the energy loss in the $Ce^{3+} \rightarrow Mn^{2+}$ energy transfer process. As for

CGZA:Ce^{3+},zTb^{3+} (z=0, 0.02, 0.04, 0.06, 0.08, 0.10, 0.12) phosphors, the external QY values vary in the range 40.9-48.9% for different Tb^{3+} doping concentrations. The CIE chromaticity diagram of the emitting phosphors CGZA:Ce^{3+},yTb^{3+},zMn^{2+} with different compositional concentrations (y and z) are displayed in Figure 14. The color tone can be tuned from (0.236, 0.499) to (0.318, 0.401) by adjusting the concentration of Tb^{3+} and from green (0.236, 0.499) to orange (0.362, 0.508) by varying the Mn^{2+} content, respectively. The inset in Figure 14 shows a series of digital photos of the selected CGZA:Ce^{3+},Tb^{3+},Mn^{2+} phosphors upon 365 nm UV lamp excitation. As depicted, Ce^{3+},Tb^{3+},Mn^{2+} activated CGZA phosphors can be potentially applied for NUV-pumped wLEDs.

4. Conclusion

In summary, we report a series of emission color-tunable $Ca_2GdZr_2(AlO_4)_3$:Ce^{3+},Mn^{2+},Tb^{3+} aluminate garnets. Utilizing Mn^{2+} and Tb^{3+} ions as energy-transfer acceptors, $Ca_2GdZr_2(AlO_4)_3$(CGZA):Ce^{3+},Mn^{2+},Tb^{3+} generates an orange emission band peaking at 572 nm and a green line peaking at 550 nm. The energy transfer from Ce^{3+} to Mn^{2+} and Ce^{2+} to Tb^{3+} in $Ca_2GdZr_2(AlO_4)_3$ host matrix is demonstrated by luminescence spectra, energy transfer efficiency, lifetimes of phosphors. The ratio of the orange emission of Mn^{2+} to the green emission of Ce^{3+} by experiment is consistent with the theoretical calculation basing on energy transfer and lifetime measurements. The energy transfer from Ce^{3+} to Mn^{2+} and Ce^{2+} to Tb^{3+} in $Ca_2GdZr_2(AlO_4)_3$ phosphors have been demonstrated to be a resonant type via a dipole−dipole mechanism. We have demonstrated that color emission as well as luminescence external QY (20.4−47.5%) can be tuned by precisely controlling the content of Ce^{3+}, Mn^{2+}, and Tb^{3+}. These results indicate that Tb^{3+}/Mn^{2+} doped $Ca_2GdZr_2(AlO_4)_3$:Ce^{3+} is a promising phosphor for application involving white light LED.

Acknowledgment.

This work is financially supported by the National Natural Science Foundation of China (Grant Nos. 21271167 and 11304309) and the Fund for Creative Research Groups (Grant No. 21221061), and the National Basic Research Program of China (973 Program, grant no 2014CB643803).

References

1 C. Feldmann, T. Jüstel, C. R. Ronda and P. J. Schmidt, *Adv. Funct. Mater.,* 2003, **13**, 511.

2 R. J. Xie, N. Hirosaki, T. Suehiro, F. F. Xu and M. Mitomo, *Chem. Mater.,* 2006, **18**, 5518.

3 J. H. Oh, S. J. Yang and Y. R. Do, *Light:Sci. Appl.* 2014, **3**, e141.

4 M. M. Shang, C. X. Li and J. Lin, *Chem. Soc. Rev.***,** 2014, **43**, 1372.

5 Z. D. Hao, J. H. Zhang, X. Zhang, X. Y. Sun, Y. S. Luo, S. Z. Lu and X. J. Wang, *Appl. Phys. Lett.,* 2007, **90(26)**, 261113.

6 J. S. Kim; P. E. Jeon, Y. H. Park, J. C. Choi, H. L. Park, G. C. Kim and T. W Kim, *Appl. Phys. Lett.*, 2004, **85(17)**, 3696.

7 X. F. Li, J. D. Budai, F. Liu, J. Y. Howe, J. H. Zhang, X. J. Wang, Z. J. Gu, C. J. Sun, R.S. Meltzer and Z. W. Pan, *Light:Sci. Appl.* 2013, **2** , e50.

8 W. J. Yang and T. M. Chen, *Appl. Phys. Lett.,* 2007, **90(17)**, 171908.

9 W. Lü, Z. D. Hao, X. Zhang, Y. S. Luo, X. J. Wang and J. H. Zhang, *Inorg. Chem.*, 2011, **50**, 7846.

10 G. G. Li, D. L. Geng, M. M. Shang, D. M. Yang, Y. Zhang, C. Peng, Z. Y. Cheng and J. Lin, *J. Phys. Chem. C.*, 2011, **115(44)**, 21882.

11 M. M. Shang, D. L. Geng, Y. Zhang, G. G. Li, D. M. Yang, X. J. Kang and J. Lin, *J. Mater. Chem.,* 2012, **22**, 19094.

12 W. Lü, N. Guo, Y. C. Jia, Q. Zhao, W. Z. Lv, M. M. Jiao, B. Q. Shao and H. P. You, *Inorg. Chem.*, 2013, **52**, 3007.

13 Z. Y. Mao, Y. C. Zhu, L. Gan, Y. Zeng, F. F. Xu, Y. Wang, H. Tian, J. Li and D. J. Wang, *J. Lumin.*, 2013, **134**, 148.

14 W. Lü, Y. C. Jia, W. Z. Lv, Q. Zhao and H. P. You, *New J. Chem.,* 2013, **37**, 3701**.**

15 M. A. Mickens and Z. Assefa, *J. Lumin.*, 2014, **145**, 498.

16 W. Lü, Y. C. Jia, W. Z. Lv, Q. Zhao and H. P. You, *Chem. Commun.,* 2014, **50**, 2635.

17 K. Li, D. L. Geng, M. M. Shang, Y. Zhang, H. Z. Lian and J. Lin,*J. Phys. Chem. C.*, 2014, **118**, 11026.

18 X. G. Zhang and M. L. Gong, *Dalton Trans.*, 2014, **43**, 2465.

19 X. Chen, P. P. Dai, X. T. Zhang, C. Li, S. Lu, X. l. Wang, Y. Jia and Y. C. Liu, *Inorg. Chem.*,

2014, **53**, 3441.

20 H. K. Liu, Y. Luo, Z. Y. Mao, L. B. Liao and Z. G. Xia, *J. Mater. Chem. C*, 2014, **2**, 1619.

21 G. Blasse and A. Bril, *Philips Res. Rep.* 1967, **22**, 481.

22 Y. Shimomura, T. Honma, M. Shigeiwa, T. Akai, K. Okamoto and N. Kijima, *J. Electrochem. Soc.*, 2007, **154**, J35.

23 A. A. Setlur, W. J. Heward, Y. Gao, A. M. Srivastava, R. G. Chandran and M. V. Shankar, *Chem. Mater.*, 2006, **18**, 3314.

24 R. Mueller-Mach, G. O. Mueller, M. R. Krames and T. Trottier, *IEEE J. Sel. Top. Quantum Electron.,* 2002, **8**, 339.

25 Y. C. Jia, Y.J. Huang, Y. H. Zheng, N. Guo, H. Qiao, Q. Zhao, W.Z. Lv and H. P. You, *J. Mater. Chem.*, 2012, **22**, 15146.

26 Y. F. Liu, X. Zhang, Z. D. Hao, Y. S. Luo, X. J. Wang and J. H. Zhang, *J. Mater. Chem.*, 2011, **21**, 16379.

27 Y. F. Liu, X. Zhang, Z. D. Hao, X. J. Wang and J. H. Zhang, *Chem. Commun.*, 2011, **47**, 10677.

28 X. H. Gong, J. H. Huang, Y. J. Chen, Y. F. Lin, Z. D. Luo and Y. D. Huang, *Inorg. Chem.,* 2014, **53**, 6607.

29 W. J. Yang, L.Y. Luo, T. M. Chen and N. S. Wang, *Chem. Mater.*, 2005, **17**, 3883.

30 M. Inokuti and F. Hirayama, *J. Chem. Phys.* 1965. **43**, 1978.

31 Z. P. Lian, J. F. Sun, L. J. Zhang, D. Z. Shen, G. Q. Shen, X. Q. Wang and Q. F. Yan, *RSC Adv.*, 2013, **3**, 16534.

32 C. F. Guo, J Yu, X. Ding, M. Li, Z. Y. Ren and J. T. Baia, *J. Electrochem. Soc.,* 2011, **158**(2), J42.

33 Y. Zorenko, V. Gorbenko, T. Voznyak, M. Batentschuk, A. Osvet and A. Winnacker, *J. Lumin.*, 2010, **130**, 380.

Figure captions:

Figure 1: XRD patterns of the CGZA:Ce^{3+},Mn^{2+} and CGZA:Ce^{3+}, Tb^{3+} samples.

Figure 2: PL and PLE spectra of CGZA:$Ce^{3+}$and CGZA:Mn^{2+} phosphors together with the reflection spectra of CGZA and CGZA:Ce^{3+} samples.

Figure 3: PLE and PL spectra of CGZA:Ce^{3+},Mn^{2+}.

Figure 4: PL spectra of Ce^{3+},Mn^{2+} co-doped CGZA various Mn^{2+} concentrations (y=0, 0.04, 0.08, 0.12, 0.16, 0.20 and 0.24) under UV excitation (λ_{ex} = 420 nm).

Figure 5: Decay curves of Ce^{3+} with different Mn^{2+} concentrations. (excited at 340 nm, monitored at 500 nm)

Figure 6: Dependence of the fluorescence lifetime of the Ce^{3+} and energy transfer efficiency on doped Mn^{2+} molar concentration in CGZA:Ce^{3+},yMn^{2+} samples.

Figure 7: Calculated and experimental ratios I_O/I_G of the orange band to the green band at different Mn^{2+} concentrations. The ratios are scaled to the maximum.

Figure 8: log{ln[$I_{D0}(t)/I_D$(t)] } vs log(t) for various Mn^{2+} contents.

Figure 9: PL and PLE spectra of CGZA:Ce^{3+}, CGZA:Tb^{3+} and CGZA:Ce^{3+}, Tb^{3+}.

Figure 10: PL spectra of CGZA:Ce^{3+}, zTb^{3+} phosphors with various Tb^{3+} content.

Figure 11: Decay curves of the Ce^{3+} fluorescence in CGZA:Ce^{3+}, zTb^{3+} samples. (excited at 340 nm, monitored at 500 nm).

Figure 12: log{ln[$I_{D0}(t)/I_D$(t)] } vs log(t) for various Tb^{3+} contents.

Figure 13:The values of the relative intensity and the external quantum yields of CGZA:Ce^{3+},yMn^{2+} (a) and CGZA:Ce^{3+}, zTb^{3+} (b) samples.

Figure 14: CIE chromaticity diagram for CGZA:Ce^{3+},Tb^{3+},Mn^{2+} phosphors, together with their corresponding photographs under a 365 nm UV lamp.

Figure 1

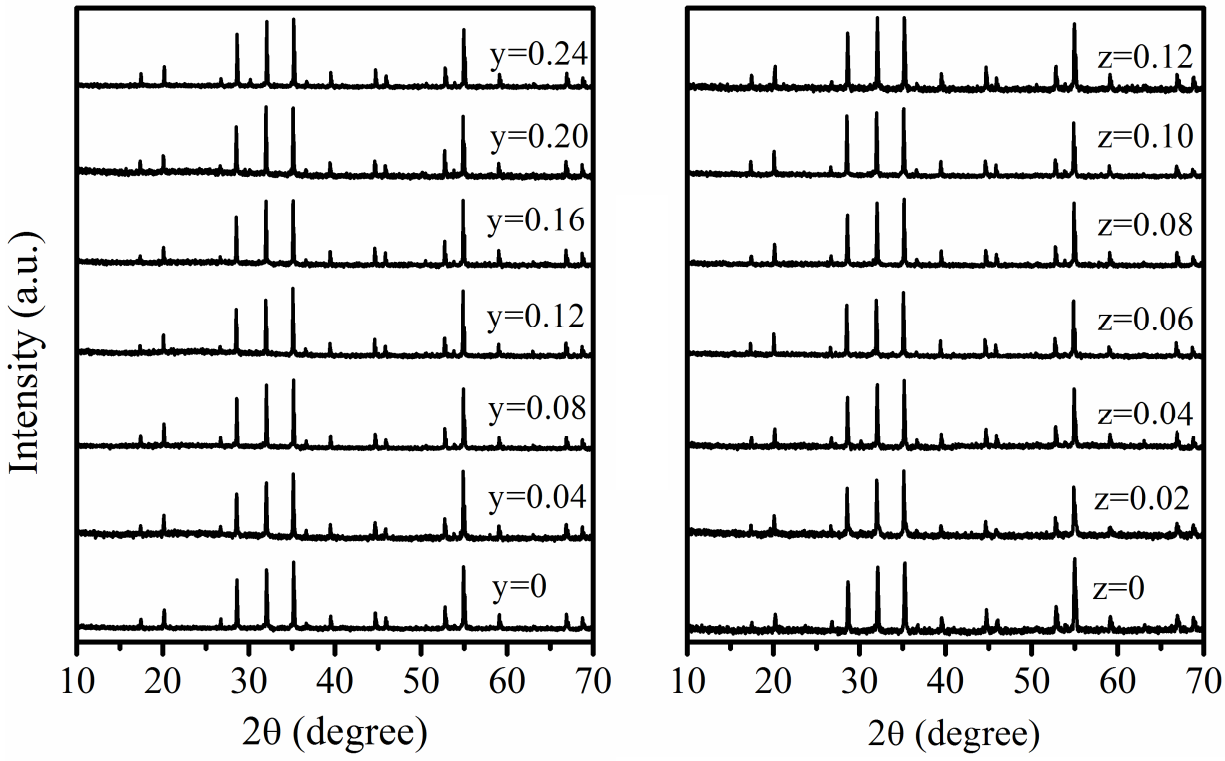

Figure 2

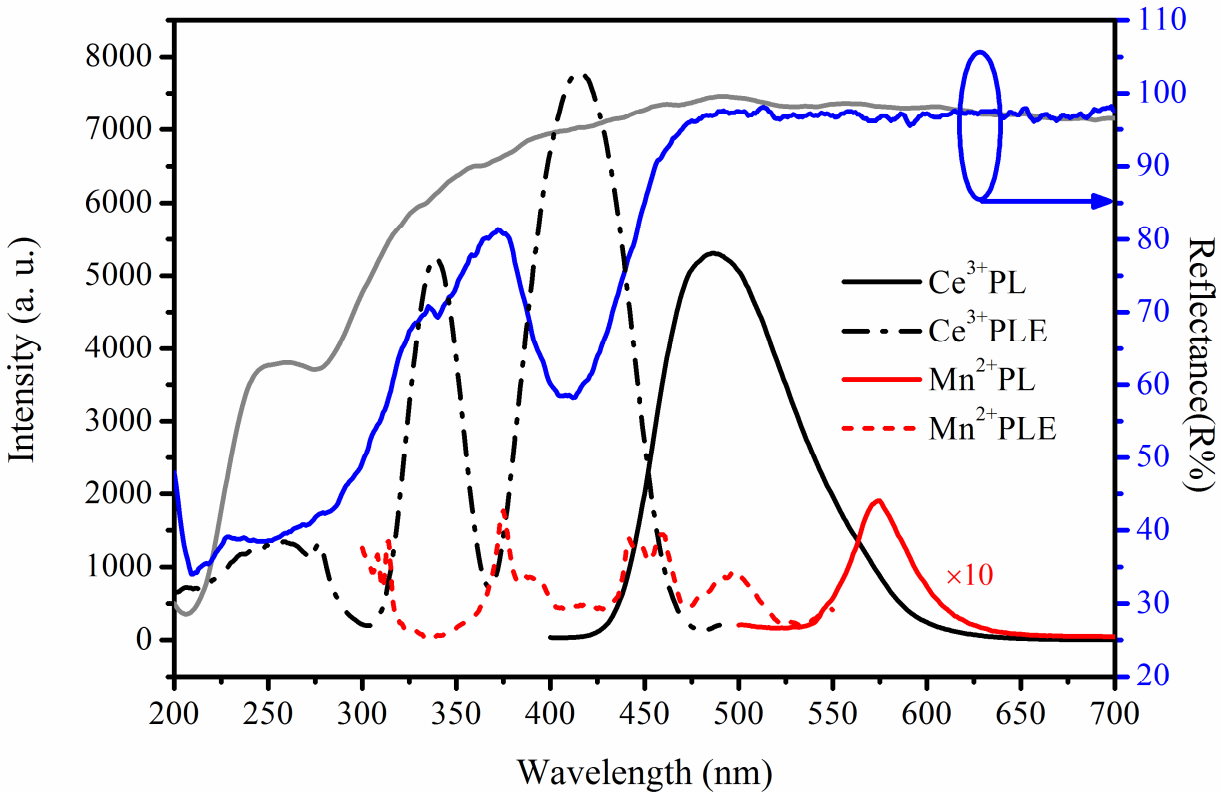

Figure 3

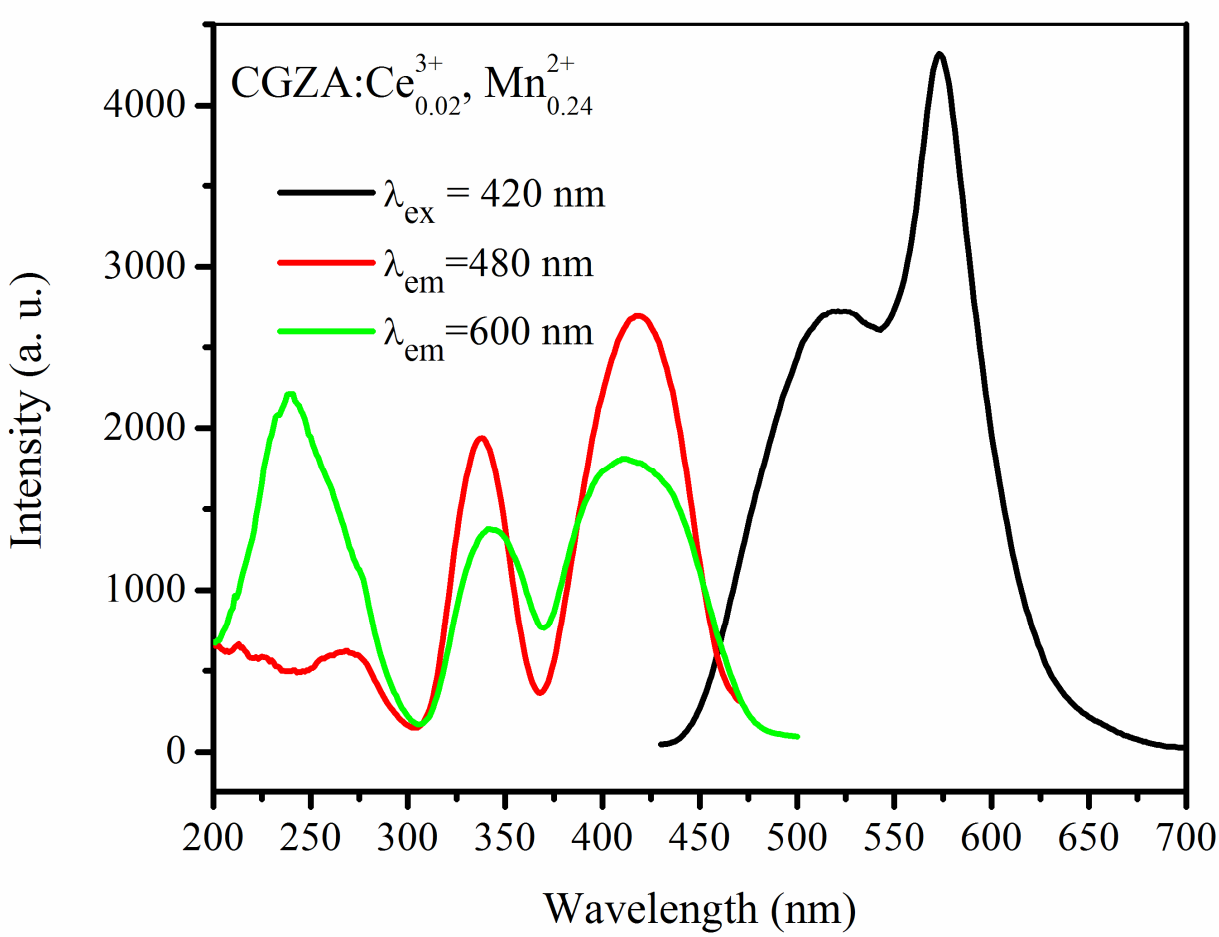

Figure 4

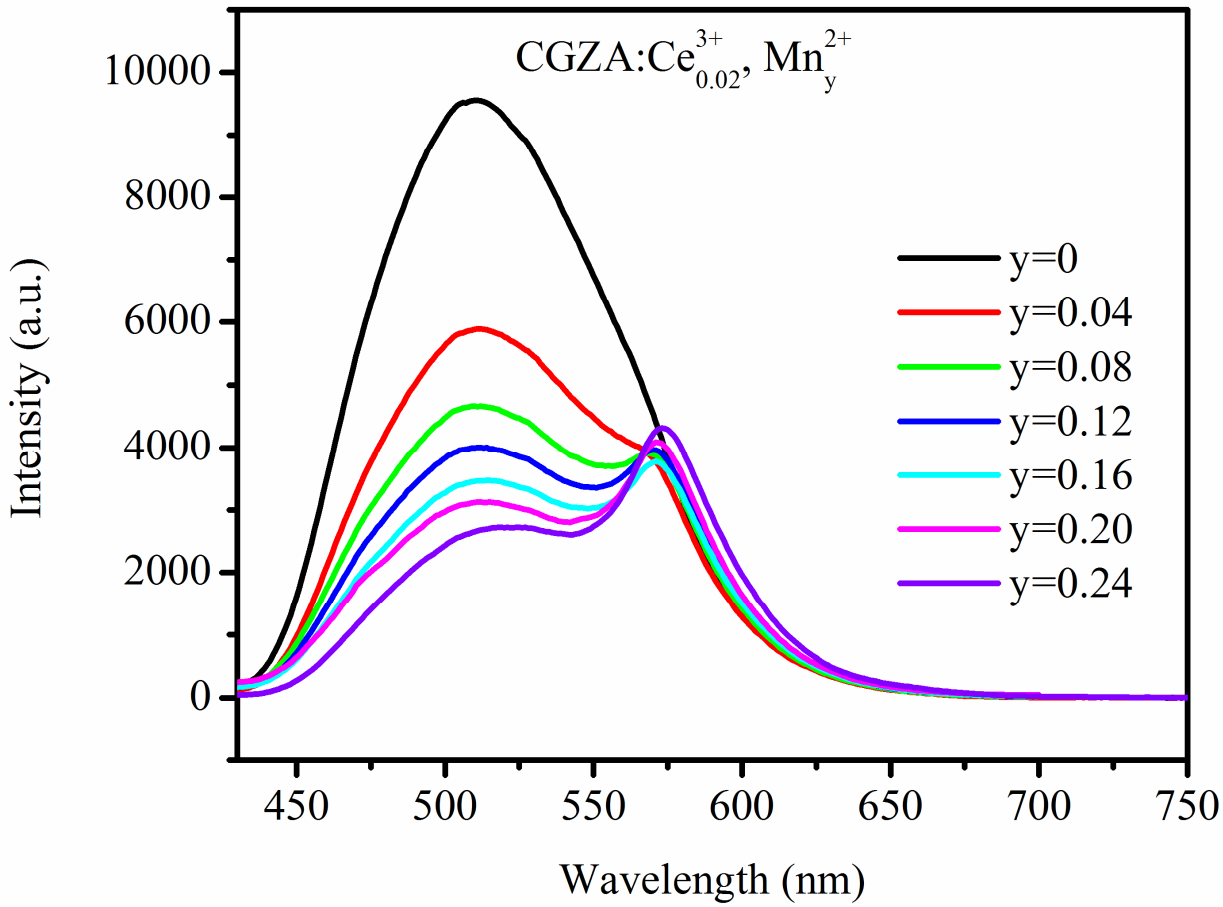

Figure 5

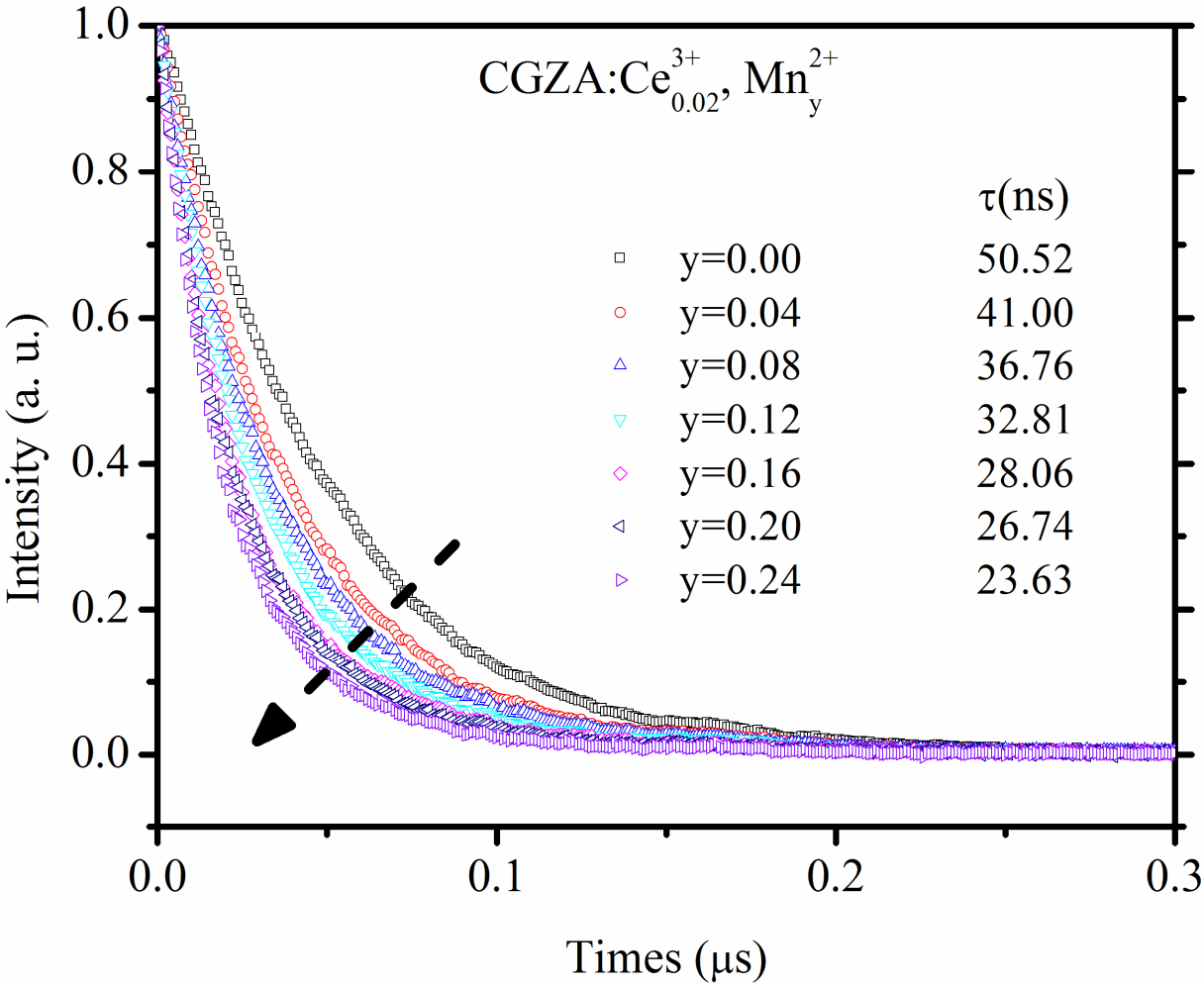

Figure 6

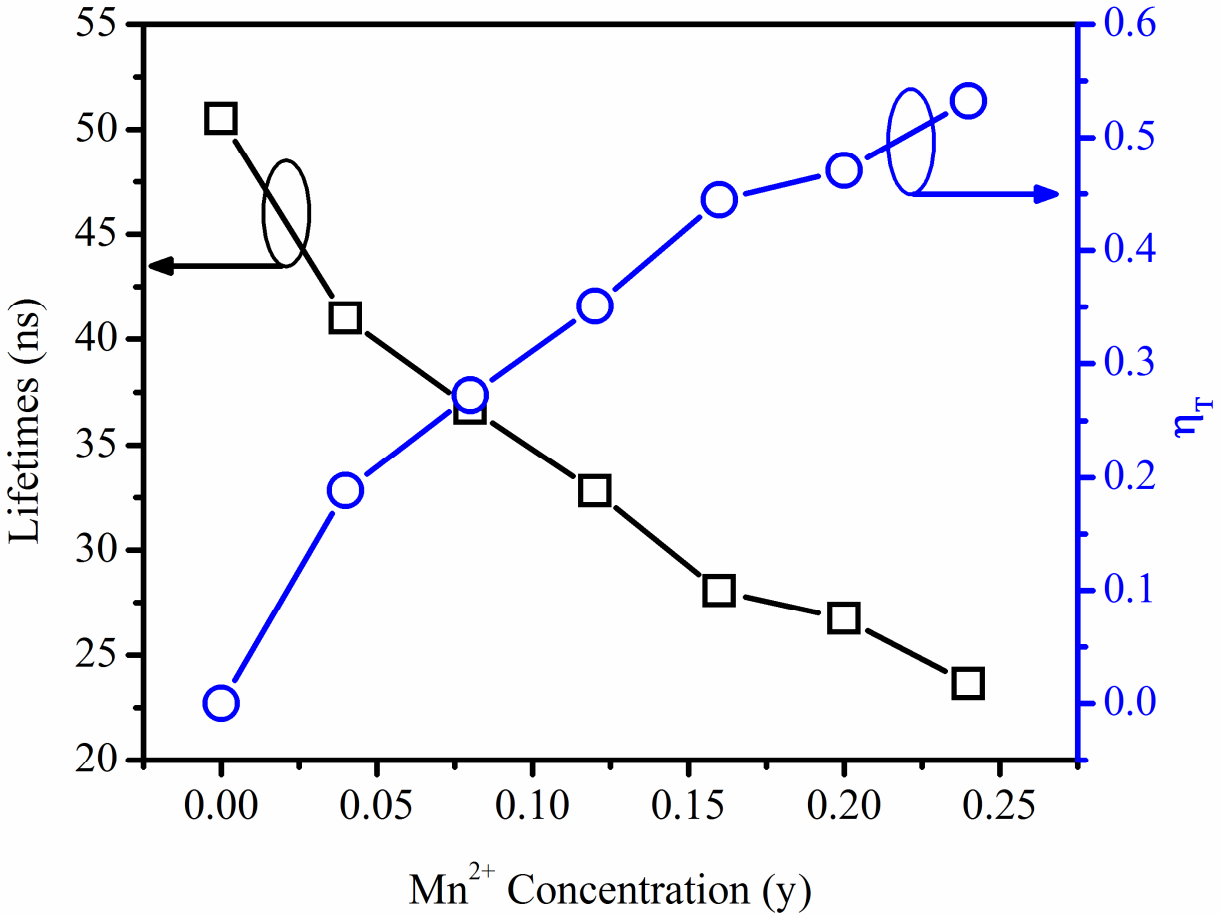

Figure 7

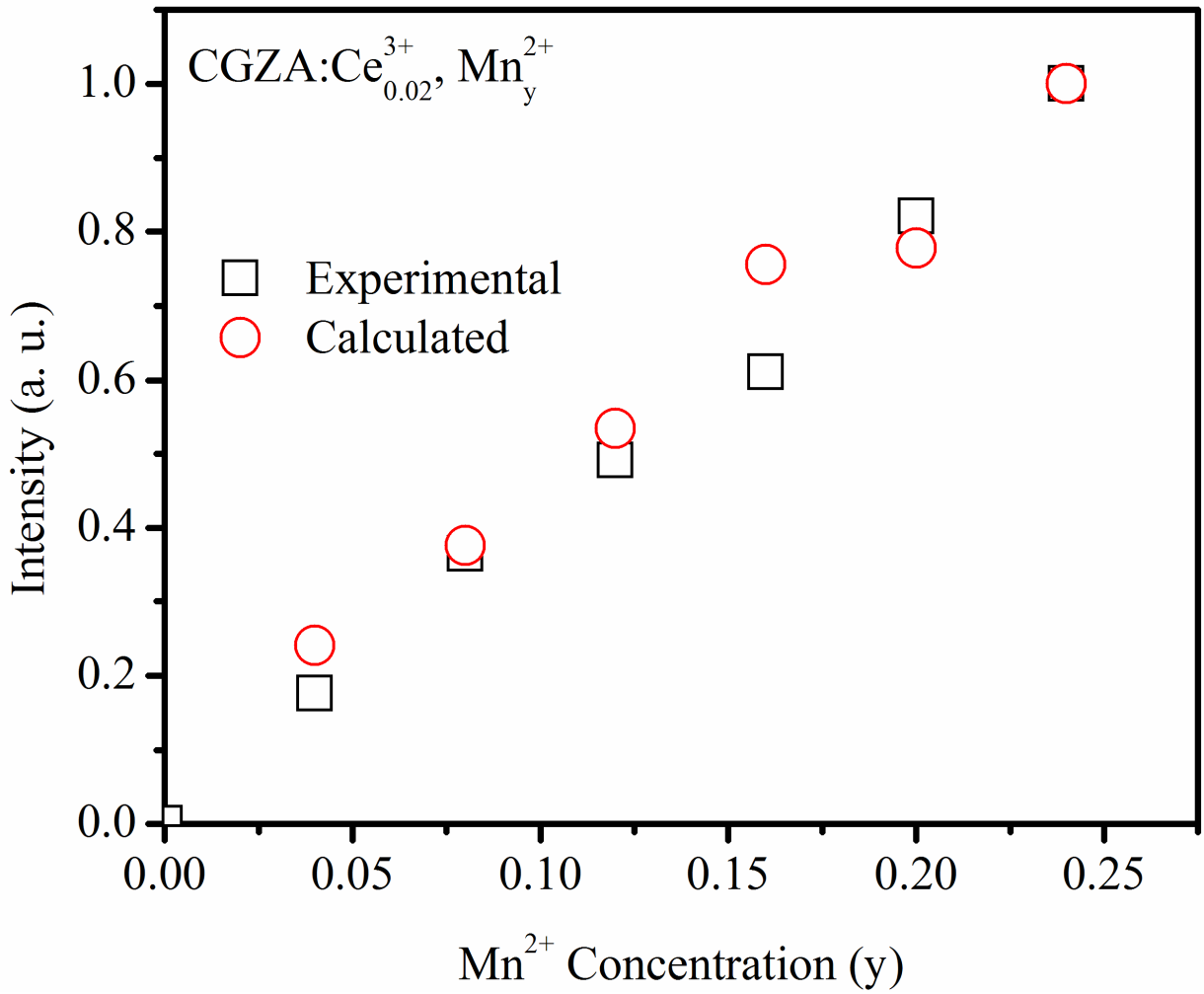

Figure 8

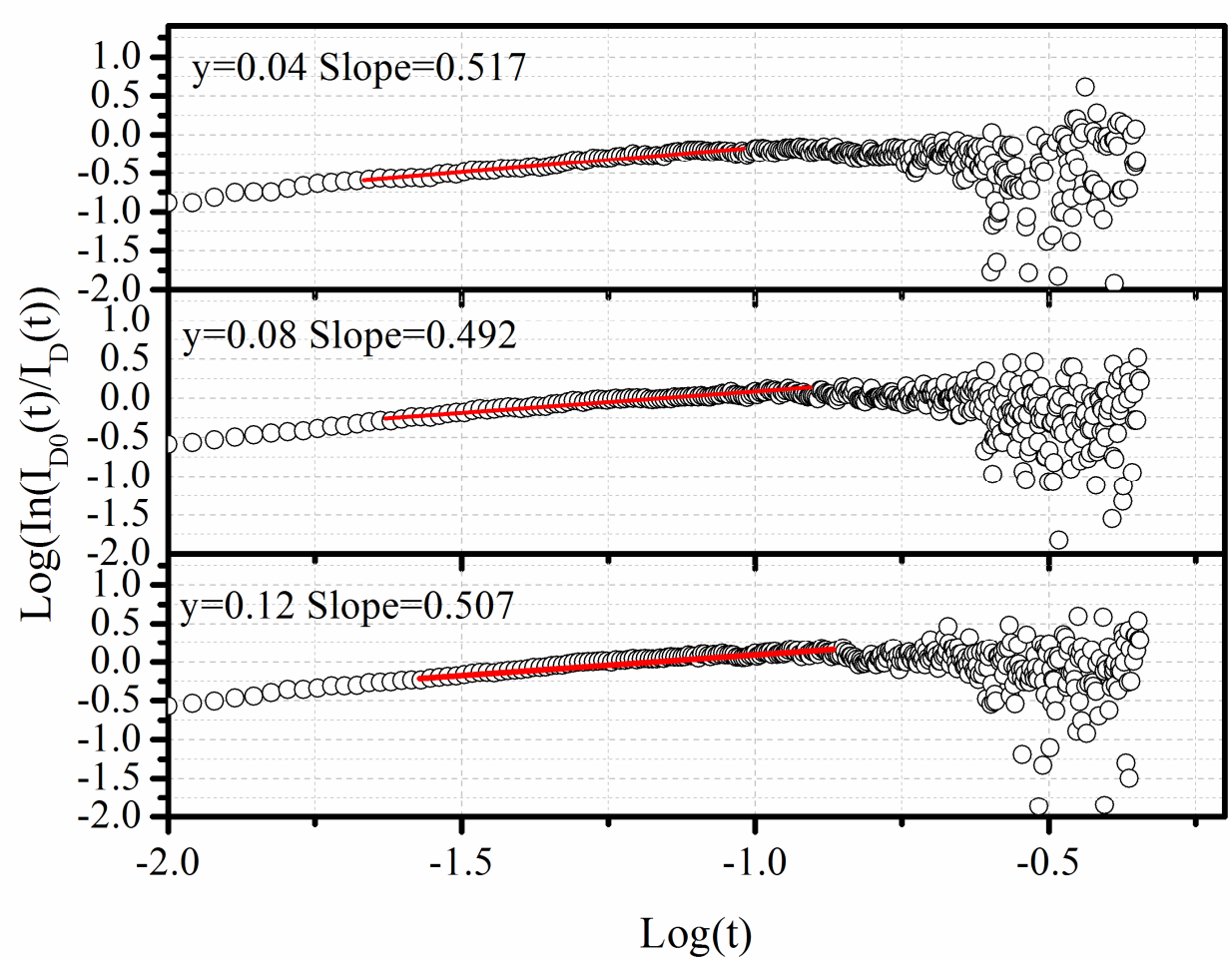

Figure 9

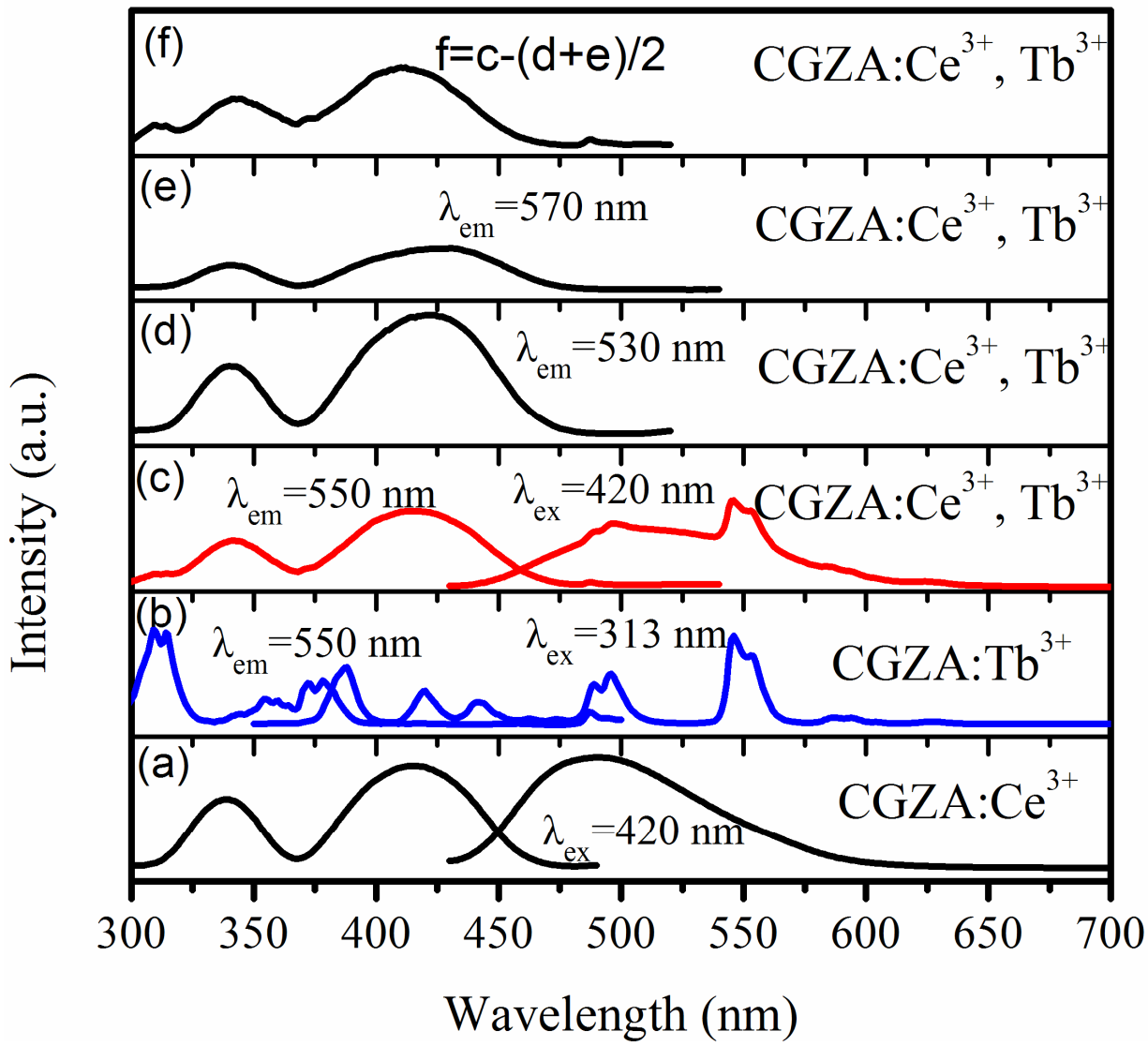

Figure 10

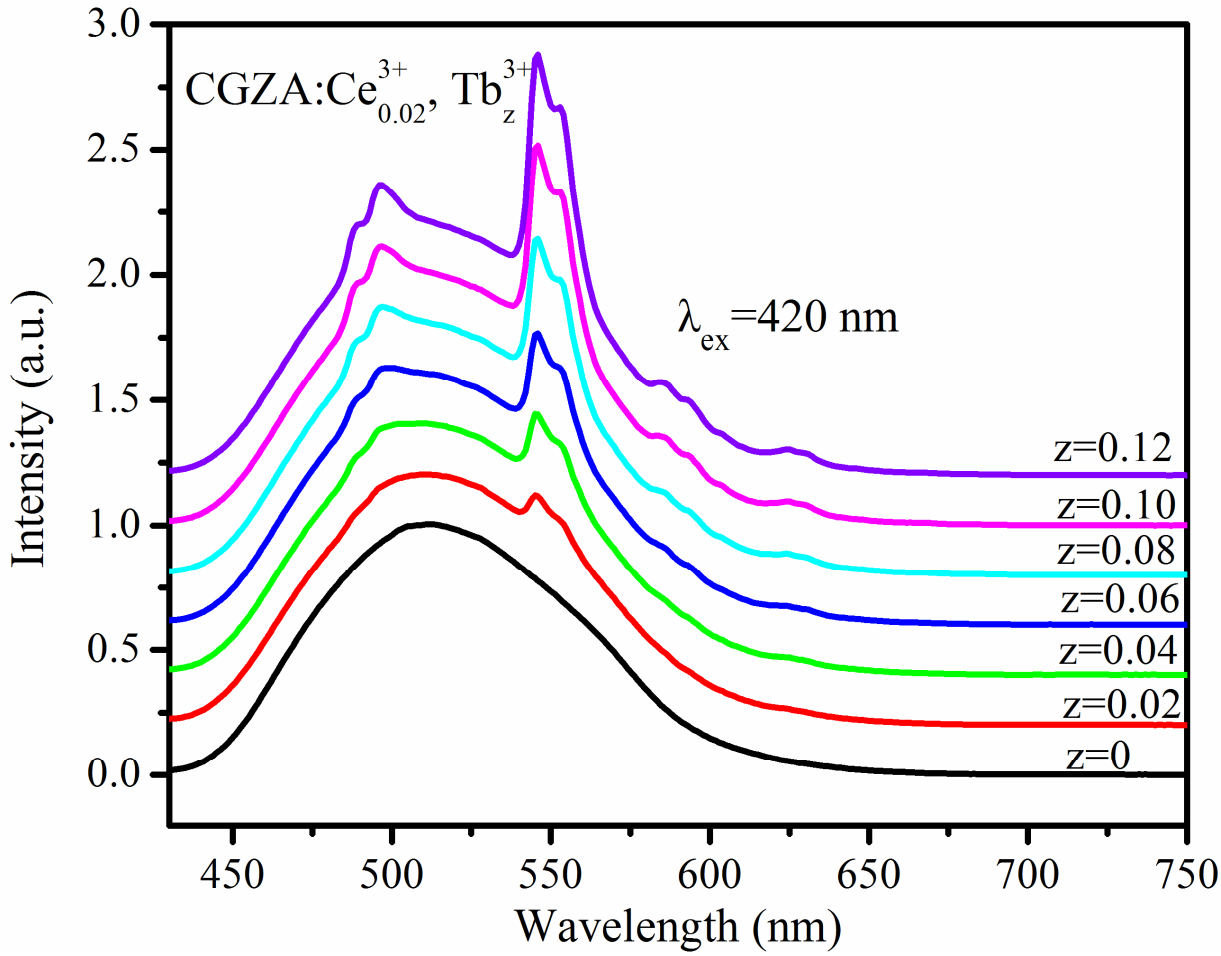

Figure 11

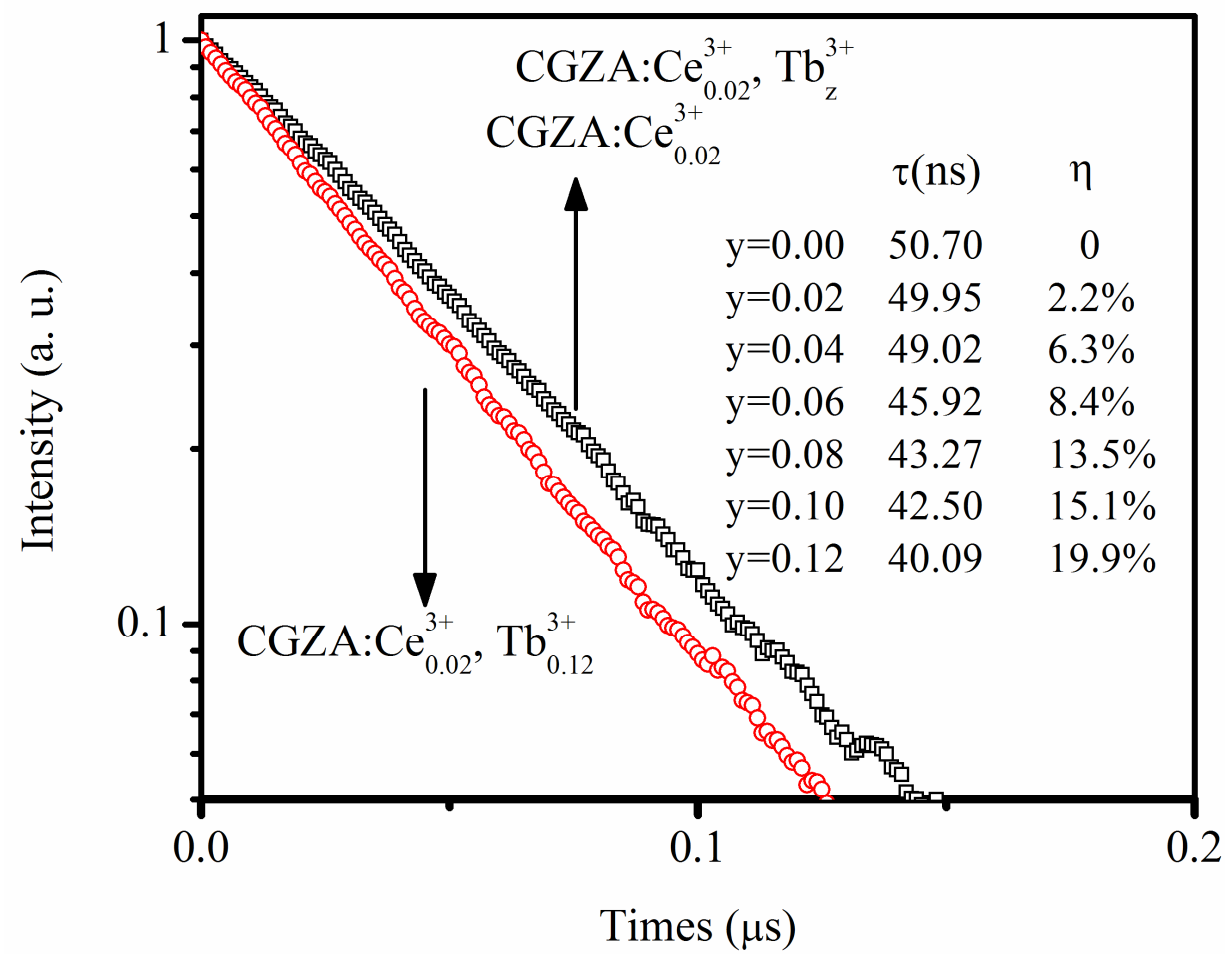

Figure 12

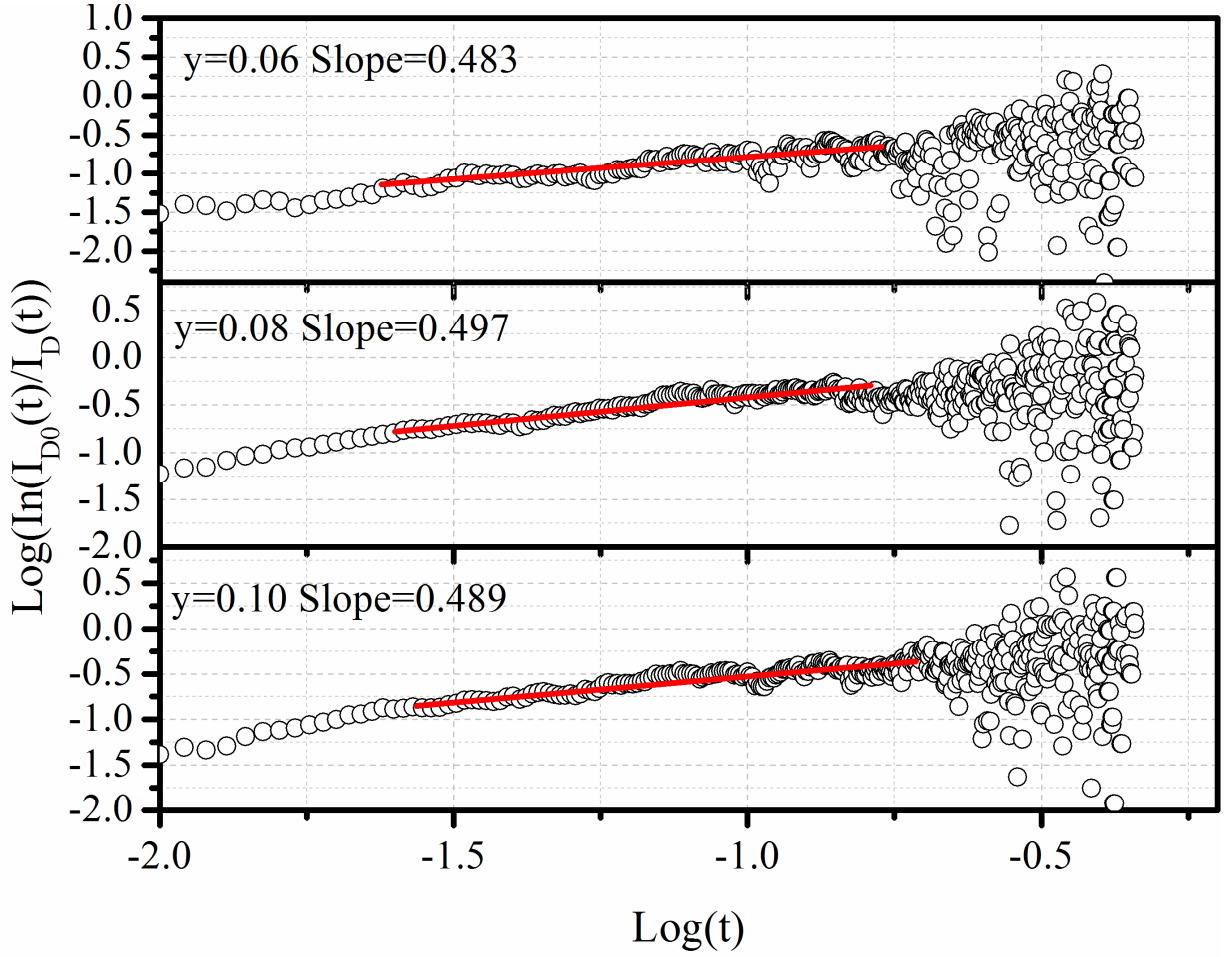

Figure 13

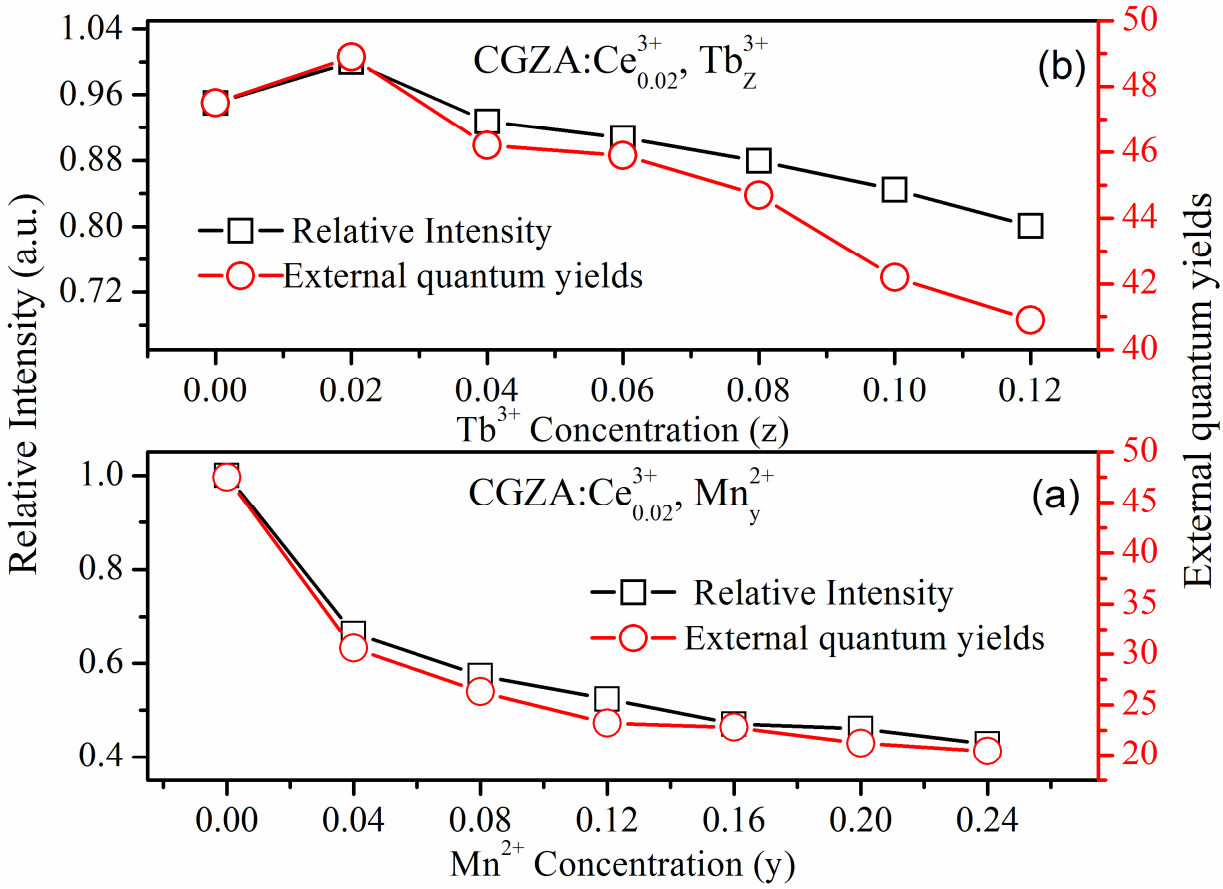

Figure 14

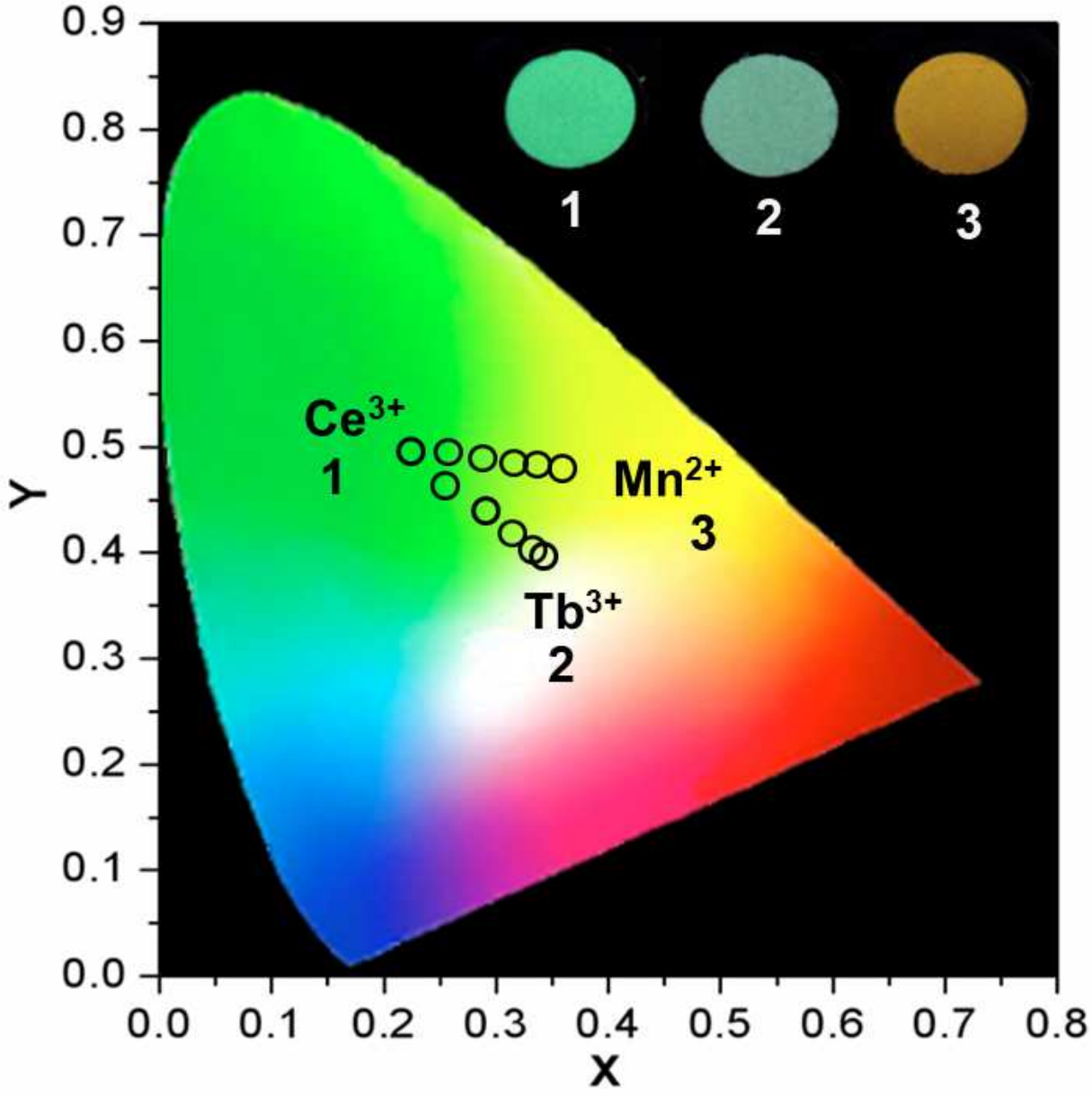

A table of contents entry

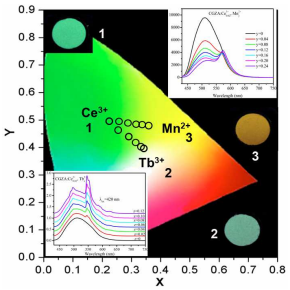

Utilizing Mn^{2+} and Tb^{3+} ions as energy-transfer acceptors, we report a series of emission color-tunable $Ca_2GdZr_2(AlO_4)_3$:Ce^{3+},Mn^{2+},Tb^{3+} aluminate garnets.